

Structure to Property: Chemical Element Embeddings and a Deep Learning Approach for Accurate Prediction of Chemical Properties

Shokirbek Shermukhamedov^{1,*}, Dilorom Mamurjonova² and Michael Probst^{1,3}

¹ Institute of Ion Physics and Applied Physics, University of Innsbruck, 6020 Innsbruck, Austria

² Tashkent Chemical Technological Institute, 100011 Tashkent, Uzbekistan

³ School of Molecular Science and Engineering, Vidyasirimedhi Institute of Science and Technology, 21201 Rayong, Thailand.

* Author to whom any correspondence should be addressed.

E-mail: shokirbek.shermukhamedov@uibk.ac.at

Abstract

We introduce the elEmBERT model for chemical classification tasks. It is based on deep learning techniques, such as a multilayer encoder architecture. We demonstrate the opportunities offered by our approach on sets of organic, inorganic and crystalline compounds. In particular, we developed and tested the model using the *Matbench* and *Moleculenet* benchmarks, which include crystal properties and drug design-related benchmarks. We also conduct an analysis of vector representations of chemical compounds, shedding light on the underlying patterns in structural data. Our model exhibits exceptional predictive capabilities and proves universally applicable to molecular and material datasets. For instance, on the Tox21 dataset, we achieved an average precision of 96%, surpassing the previously best result by 10%.

1 Introduction

Due to their effectiveness in fitting experimental data and predicting material properties, machine learning models have found extensive applications in research on batteries [1,2], supercapacitors [3], thermoelectric [4] and photoelectric [5] devices, catalysts [6] and in drug design [7]. In a 'second wave', deep learning models (DLMs) have exhibited remarkable potential in advancing the field of chemical applications. So-called Word2vec [8] DLMs have been used for processing textual chemical data extracted from academic articles. By representing chemical formulas as embeddings or vectors, non-obvious connections between compounds and chemical properties can be discovered. For instance, the mat2vec [9] NLP model was able to predict materials with good thermoelectric properties, even when these materials and their properties were not explicitly named in the original papers. Other NLP-inspired models, such as Bag of Bonds [10], mol2vec [11], smiles2vec [12], SPvec [13], have used unsupervised machine learning and have been applied to chemical compound

classification tasks, achieving remarkable results. These models hold immense potential for accelerating the discovery and the design of materials with tailored properties.

In this regard, the type of input data is crucial for ML models. In chemistry, this could be chemical text data, like in mat2vec, or structural data. Chemical texts make it possible to use reference information of a compound [14], such as molecular weight, melting point, crystallization temperature, and element composition. These types of inputs can, in turn, be used by general deep learning models, with ELMO, BERT, and GPT-4 being the most famous examples. However, such models cannot directly capture 3D information from structural files.

One of the most common types of input data used for ML-based approaches is structural representation, which provides valuable information about the atomic environment of a given material. However, text-based data does not normally capture important structural features, such as interatomic distances. Structural information is crucial for predicting material properties, as it is key to all pertinent physical and chemical characteristics. This can be understood in the same sense as the Born-Oppenheimer approximation, in short, states that atomic coordinates (and from them the potential energy) are all that is needed in chemistry. The challenge of linking structural information to material properties is commonly referred to as the "structure to property" task. Overcoming this challenge has the potential to greatly enhance our ability to predict and design novel materials with desired properties.

Structure can be translated into property by graph neural networks (GNN) or high-dimensional neural networks (HDNN) formalisms. GNNs transform graphs of molecules (or compounds) into node and edge embeddings, which can then be used for state-of-the-art tasks [15–22]. GNNs are efficiently used for both chemical classification and regression tasks. However, as the size and complexity of molecular graphs increase, the computational requirements for GNNs also grow. Handling large graphs with many atoms or intricate structures can pose scalability challenges, both in terms of memory usage and computer time. HDNNs based on converting Cartesian coordinates of atoms to continuous representations use techniques like the smooth overlap of atomic positions (SOAP) [23], the many-body tensor representation (MBTR) [24], or the atomic centered symmetry functions (ACSF) [25] to achieve the same goal. Message passing neural networks (MPNN) are a subgroup of HDNN that use atomic positions and nuclear charges as input. The PhysNet [26] model serves as a typical example. In this model, atomic embedding encodes the atomic identifier into vector arrays, which are first initialized randomly and optimized during training.

HDNNs demonstrate excellent performance on regression tasks. However, in classification tasks GNNs dominate. Moreover, a disadvantage of HDNNs is their susceptibility to overfitting and their

computational complexity. As the dimensionality increases, the possibility of overfitting rises due to the larger number of parameters, while also the training time increases.

Despite the increasing use of deep learning in computational chemistry, many aspects of NLP models have yet to be fully explored. One of them is the attention mechanism [27], which allows the model to focus on specific parts of the input data when making predictions. It works by assigning different levels of importance, or attention, to different elements in the input sequence. Additionally, the so-called transformer approach, commonly known for its successful application in chemical GNNs, has not been fully extensively applied to HDNNs. The transformer consists of two distinct components: an encoder responsible for processing the input data and a decoder responsible for generating task-related predictions. In this paper, we introduce a new deep learning model for chemical compounds that utilizes both of these approaches. Specifically, our model incorporates local attention layers to capture properties of local atomic environments and then utilizes a global attention layer to make weighted aggregations of these atomic environment vectors to create a global representation of the entire chemical structure. While the attention mechanism has been previously used in graph neural networks [28], this work introduces an atomic representation deep learning model that can be applied to a wide range of tasks. From its components, we call this model 'elEmBERT' (**e**lement **E**mbeddings and **B**idirectional **E**ncoder **R**epresentations from **T**ransformers).

In summary, the main aspects of our work are:

- a. We use a transformer mechanism for binary and multilabel classification based on structural information.
- b. Our model is flexible, fast and can be easily adapted to different types of datasets.
- c. Benchmarks show the state-of-the-art performance of our model for a variety of material property prediction problems, both involving organic and inorganic compounds.

2 Methods

As input to the neural network (NN), we use atomic pair distribution functions (PDFs) and the atom types that compose the compounds. The PDF represents the probability of finding an atom inside a sphere with a radius r centered at a selected atom [29]. To prepare the training data, we calculate PDFs employing the ASE library [30] with a cutoff radius of 10Å [31]. The second input for the NN consists of element embedding vectors. To achieve this, all elements in all compounds are mapped to integers (typically using the nuclear charge), creating an elemental vocabulary of size $V_{size}=101$. These embeddings are then passed to the BERT module.

BERT (Bidirectional Encoder Representations from Transformers) is a deep learning architecture originally designed for natural language processing (NLP) tasks. It employs a bidirectional transformer encoder to capture word context in sentences, allowing it to generate accurate text representations. BERT employs masked language modeling (MLM), where some tokens in a sentence are masked or replaced with a [MASK] token, and the model is trained to predict the original word based on the surrounding context.

2.1 Model architecture

Our model is illustrated in Fig. 1. It can use various combinations of embedding sizes, encoder layers, and attention heads. In chemical applications, the atomic composition of a compound can be equated to a sentence, with individual atoms serving as constituent tokens. Leveraging this analogy, we introduce four new tokens to the vocabulary: [MASK] for MLM, [UNK] for unseen tokens, [CLS] for classification, and [SEP] for separating two compounds.

In standard BERT models so-called positional embeddings play an important role by encoding the order of tokens in a sequence, which allows the model to capture sequential relationships between tokens. Since the Transformer approach is inherently permutation-invariant – treating different permutations of the same input sequence identically – there is no explicit encoding of token order. As well, in chemical compounds the order of atoms does not affect the properties of the entire compound. Correspondingly, in our implementation, positional embeddings are intentionally omitted to preserve permutation invariance.

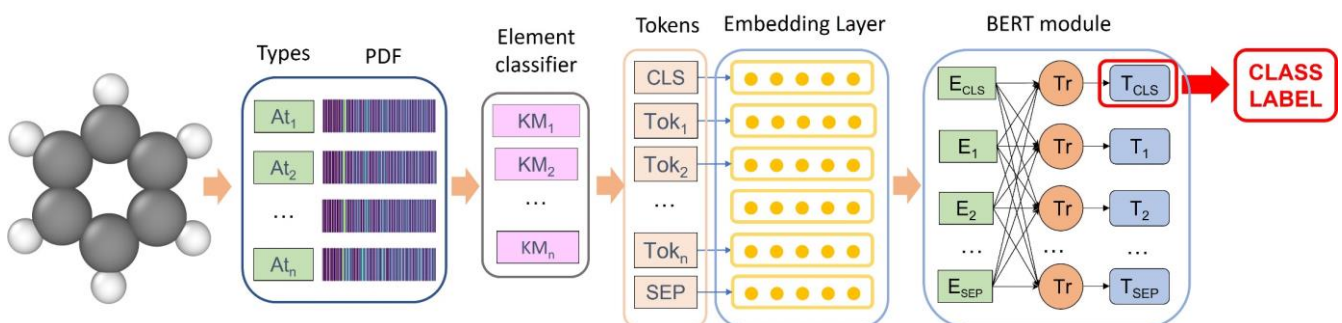


Figure 1. Classification Model Architecture: The initial step involves computing the pair distribution function for each element based on atom positions within the chemical compound. This information is then passed through the classifier model. Subsequently, the resulting sub-elements are converted into tokens, with additional tokens incorporated before input into the BERT module. The [CLS] token output vector from BERT is used for the classification task.

In chemical compounds, elements may exhibit varying oxidation states or formal charges, indicating the relative electron loss or gain during reactions. The interactions between these elements are non-uniform and follow specific patterns based on their neighboring atoms. For inorganic substances,

these interactions typically appear as ionic interactions, signified by the oxidation state, while in organic substances, covalent bonding is prevalent.

To establish a universal criterion for categorizing these interactions, we group elements in our training dataset into “sub-elements” based on the local environment of atoms in compounds. We use the PDF and the oxidation state of each element to determine the number of possible sub-elements. It is crucial to note that information about the specific interaction type in molecular structures is often missing, which can lead to algorithmic errors. Recognizing that bond length contains information about interactions, we used unsupervised clustering to categorize elements. This approach is similar to the methods used manually in the development of classical force fields [32].

We evaluated several algorithms and ultimately selected the k-means algorithm due to its speed and simplicity. For fitting, we utilized structures from the Crystallography Open Database (COD) [33,34]. Detailed information is provided in Appendix A. To illustrate the effectiveness of our approach, we present examples of sub-element classifications for lithium (Li) and magnesium (Mg) atoms. In these examples, Li and Mg atoms are classified into two and three groups, accordingly. These t-SNE (t-distributed stochastic neighbor embedding) plots offer a visual summary of the relationships and distinctions between different sub-elements, demonstrating the capabilities of our classification algorithm.

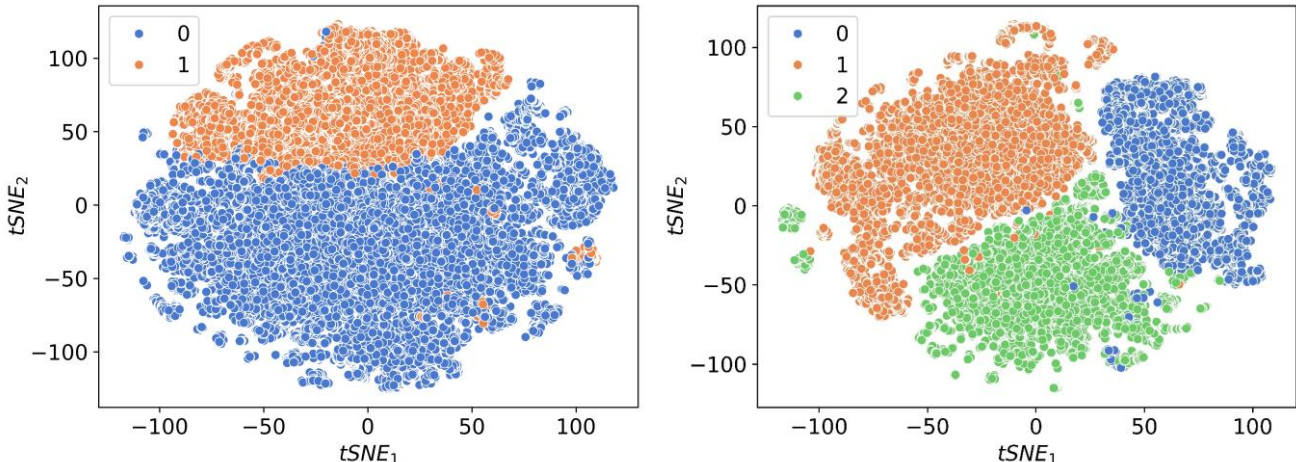


Figure 2. Sub-element classification and t-SNE Plots for Li (left) and Mg (right) atoms. tSNE plots obtained from PDF of atoms from COD dataset.

We fitted an individual model for each element in our dataset, resulting in a total of 96 models. The final dictionary size was $V_{size}=565$. Examples of such differentiation are presented in Fig. 3.

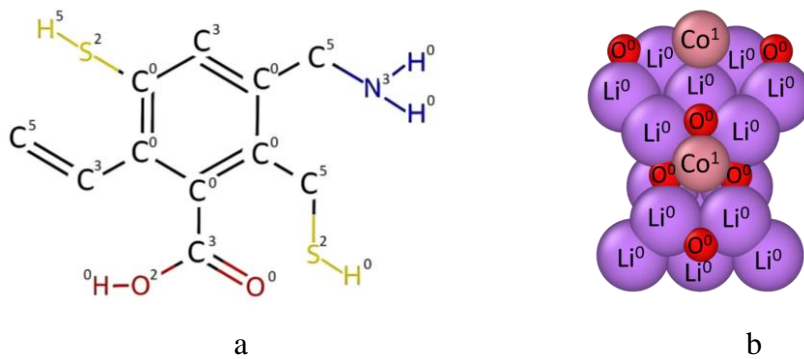


Figure 3. Two examples illustrating the division of elements into sub-elements based on their environment: a hypothetical organic compound (a) and Li_8CoO_6 (b) crystal with ID mp-27920. The numbers at the top right of elements correspond to sub-elements.

2.2 Datasets

We trained our elEmBERT model to perform various classification tasks. To do this, we used the [CLS] token and added an additional layer to the BERT module with the same number of neurons as there are classes in the dataset. Our first task involved using the Materials Project (MP) metallicity dataset to predict the metallicity of materials based on crystal structure information [35,36]. Next, we employed a portion of the datasets gathered for the CegaNN model [37]. This led us to undertake a classification task known as the Liquid-Amorphous (LA) task, which revolves around distinguishing between liquid and amorphous phases of silicon (Si). The LA dataset comprises 2,400 Si structures, evenly divided between amorphous and liquid phases (50% each). Importantly, these Si structures lack symmetry and differ solely in terms of density and coordination number. In addition to these tasks, we evaluated the elEmBERT model's ability to classify material polymorphs across different dimensionalities, specifically clusters (0D), sheets (2D), and bulk structures (3D). Carbon, with its wide range of allotropes spanning these dimensionalities, served as an excellent system for assessing the efficiency of our network model in dimensionality classification (DIM task). The DIM dataset contained 1,827 configurations. Finally, we ventured into characterizing the space group of crystal structures, encompassing a total of 10,517 crystal structures distributed among eight distinct space groups (SG task) [38].

Expanding beyond inorganic material datasets, we incorporated organic compounds, which greatly outnumber their inorganic counterparts. This expansion encompasses an extended range of properties, including biochemical and pharmaceutical aspects. To rigorously validate our model, we turned to benchmark datasets from MoleculeNet [39], specifically BBBP (Blood-Brain Barrier Penetration), ClinTox (Clinical Toxicity), BACE (β -Secretase), SIDER (Side Effect Resource) [40], and Tox21. Notably, the Tox21 and SIDER datasets encompass 12 and 27 individual tasks, respectively, each corresponding to specific toxicity predictions. These datasets cover a diverse array of chemical

compounds and provide a comprehensive assessment of our model's predictive performance for binary properties or activities associated with organic molecules. In this context, a positive instance signifies that a molecule possesses a specific property, while a negative instance indicates its absence. The MoleculeNet dataset primarily comprises organic molecules represented in Simplified Molecular Input Line Entry System (SMILES) format. For purposes of analysis, we converted these SMILES formulas into the standard XYZ format using the Open Babel software [41] and RDKit package [42]. To evaluate our model's performance, we employed the 'Receiver Operating Characteristic - Area Under the Curve' (ROC-AUC) metric, a common measure for assessing binary classification quality. ROC-AUC quantifies the model's ability to differentiate between positive and negative classes based on predicted probabilities.

2.3 Training procedure

In the following sections, we will present the results of prediction models with specific parameters, including an embedding size of 32, 2 attention heads, and 2 layers. These parameter choices have been identified as optimal across all datasets considered in this study. We explored two model versions, V0 (where the K_m block is omitted) and V1, as discussed previously. These models were implemented using Keras [43] and were trained with eight k-fold splitting. This procedure is responsible for the splitting of the dataset and the initiation of model weights. We split the datasets into three subsets: the training set, the validation set, and the test set, with an 80:10:10 ratio. We employed the categorical crossentropy loss function in conjunction with the Adam optimizer, setting the learning rate at 0.001. The batch size was set to 128 for the MP task and 32 for the other datasets. The number of epochs was two and four times the batch size, respectively.

3 Results

The ROC-AUC values reported in Table 1 are based on the test set. This table provides clear evidence that the efficiency of predictions improves as the number of subtypes increases, particularly for inorganic compounds. In the LA task, using single-element inputs results in only 50% accuracy, which is comparable to random guessing. However, incorporating sub-elements significantly enhances the performance, leading to an impressive ROC-AUC of 0.98. Our approach also demonstrates improved scores across other datasets. In the subsequent sections, we will delve into each dataset, from Matbench to Toxic21, and examine the elEmBERT-V1 model in more detail, providing comprehensive insights into the predictions.

Table 1. Performance of different models applied to datasets (Matbench to TOXIC21) used in this work. A Bold font indicates the best performance and an underline represents the second-best performance, and the last column presents previous results obtained from other models. V0 represents models that use chemical element embeddings, while V1 uses sub-element embeddings as input for the BERT module.

BENCHMARK	V0	V1	BEST
MP METALLICITY	<u>0.961 ± 0.001</u>	0.965 ± 0.001	0.950 [44]
SG	0.945 ± 0.000	<u>0.952 ± 0.000</u>	1 [37]
LA	0.500 ± 0.000	<u>0.983 ± 0.003</u>	1 [37]
DIM	0.866 ± 0.008	<u>0.958 ± 0.003</u>	1 [37]
BACE	0.732 ± 0.011	<u>0.789 ± 0.005</u>	0.888 [45]
BBBP	0.903 ± 0.010	<u>0.909 ± 0.008</u>	0.932 [45]
CLINTOX	0.962 ± 0.003	<u>0.959 ± 0.005</u>	0.948 [46]
HIV	0.982 ± 0.001	<u>0.972 ± 0.000</u>	0.776 [47]
SIDER	0.778 ± 0.008	<u>0.773 ± 0.008</u>	0.659 [45]
TOX21	<u>0.965 ± 0.001</u>	0.967 ± 0.001	0.860 [46]

3.1 MP metallicity

In this task, the objective is to predict or estimate whether a material is metallic or non-metallic based on its electronic structure. Figure 4a illustrates the confusion matrix and presents the performance of the elEmBERT-V1 model in classifying MP metallicity. The dataset for this task comprises 106,113 samples of training structures and 21,222 samples of test structures. Our trained model achieves a binary accuracy of approximately 0.91 and an AUC of 0.965 on the test set.

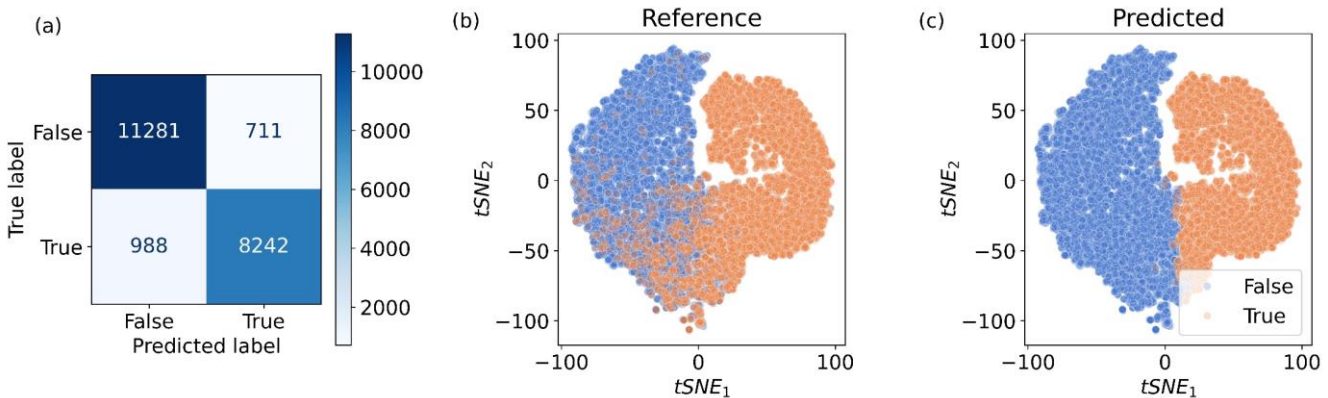


Figure 4. Confusion matrix (a) and visualization of [CLS] token embeddings for the MP metallicity dataset for the reference (b) and predicted (c) datasets: blue circles denote negative labels (not metal) and orange dots represent positive labels (metal).

In Figure 4b, the t-SNE plot shows the embeddings of the entire reference dataset, categorized by labels, revealing a smooth differentiation among labels within the feature space. Figure 4c demonstrates how our model classifies the reference dataset. It is evident that the classification models create a clear separation in the feature space, in contrast to the diffuse boundary in the reference dataset. The primary errors are located at the boundary, where the model sometimes struggles to effectively capture the diffusive behavior. The metallicity prediction task highlights elEmBERT's remarkable capability to characterize these binary properties of crystals. The results surpass the capabilities of previously published models, including those of GNNs.

3.2 LA, DIM and SG

This section presents the results obtained from benchmarks conducted for the CegaNN model, beginning with a focus on the LA classification task. Fig. 5a and 5b show the embedding representation of Si structures based on their labels, reduced through the t-SNE algorithm. Our model effectively segregates the structures into distinct clusters, with two clusters clearly corresponding to their respective classes. However, one cluster exhibits intermixing of structures, which challenges accurate recognition by the model.

The confusion matrices shown in Fig. 5c-e provide insights into the performance of the elEmBERT-V1 model across the LA, DIM, and SG datasets. The model achieves a high ROC-AUC of approximately 0.958 on the DIM task's test set and a slightly higher value of 0.968 on the SG dataset. These confusion matrices illustrate the model's ability to identify and categorize each structure accurately. It is worth noting that the model faces challenges in distinguishing the bcc (229) structure from others in the SG dataset. This challenge arises from the structural similarities between the bcc structure and others, resulting in identical geometrical representations unless the orientational order of the particles is considered.

While the CegaNN model achieves approximately 100% efficiency in this benchmark, our model does not reach this level of performance. Nonetheless, it demonstrates strengths in terms of versatility, speed, and simplicity for this benchmark as well.

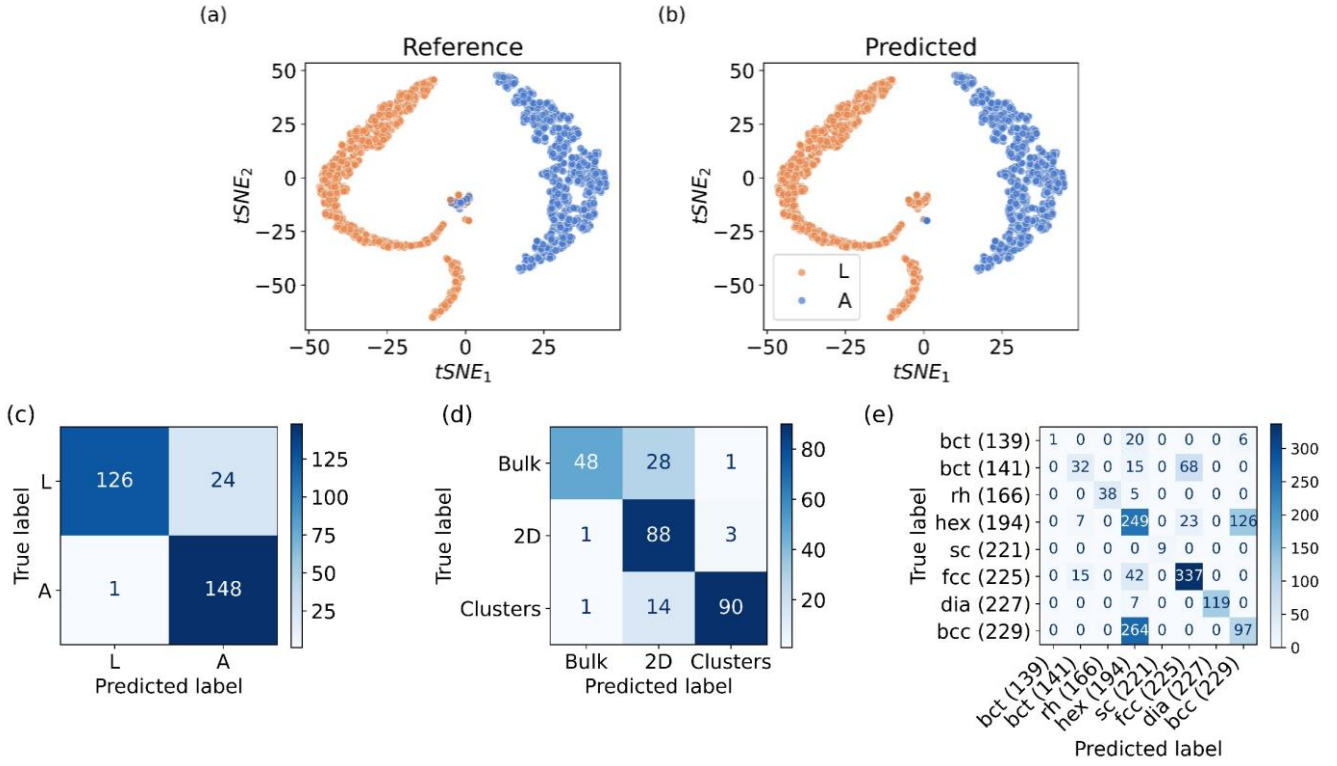


Figure 5. Top row: Visualization of [CLS] Token Embeddings for the LA Dataset: a) reference labels and b) predicted labels. The embeddings are represented using blue circles for liquid phase labels and orange dots for amorphous labels. Bottom row: Confusion matrix analysis of the LA (c), Dim (d), and SG (e) datasets.

3.3 Toxic21

The Tox21 dataset is a collection of chemical compounds evaluated for their toxicity against a panel of 12 different biological targets. With over 8,000 compounds, it serves as a valuable resource for predicting the toxicity and potential adverse effects of various chemical compounds. Our model, trained on the Tox21 dataset, demonstrated impressive performance, achieving an average AUC of 0.96 across all 12 toxicity prediction tasks [39]. The results of these individual tasks are presented in Table 2, enabling a comprehensive evaluation of the model's performance on each toxicity prediction within the Tox21 dataset.

Comparing our results with those of the Meta-Molecular GNN (MMGNN) model [22] highlights the significant advantages of our approach. Fig. 6 shows the confusion matrix of the test set and the t-SNE projection representing the features of the sr-mmp task in the Tox21 dataset. As shown, our model predicts distinct patterns in the t-SNE projections, with each label value occupying a specific region (Fig. 6b). The molecular embedding visualizations are also available in the MMGNN model report for the sr-mmp task [22]. In contrast, our feature space exhibits more structure, with positive values being less dispersed across all compounds. Our model primarily has only a few points that are significantly distant from the positive value region. Both elEmBERT models successfully identify

the boundary between these two classes and make predictions (Fig. 6c). Errors primarily arise from diffuse boundary regions and points located far from the true cluster. This observation holds true for all tasks within the Tox21 dataset.

Table 2. ROC-AUC performance of different tasks from the Tox21 dataset. MMGNN denotes the prior top-performing results [22]. The last column presents the eLemBERT model's average performance across all tasks. The Bold entry signifies the highest performance, while underlined values indicate the second-best performance.

MODEL	NR-	NR-	NR-	NR-	NR-	NR-	NR-	SR-	SR-	SR-	SR-	SR-	AVE	
	AHR	AR-	AROM	AR	ER-	ER	PPAR-	ARE	ATAD5	HSE	MMP	P53		
	LBD		LBD		GAM									
V0	0.955	0.987	0.980	0.983	0.978	0.932	0.988	0.913	0.985	0.974	0.974	0.938	0.972	0.965
V1	0.961	0.989	0.979	0.982	0.978	0.935	0.986	0.913	0.983	0.974	0.946	0.973	0.967	
MMGNN	-	-	-	-	-	-	-	-	-	-	0.748	0.804	0.790	0.781

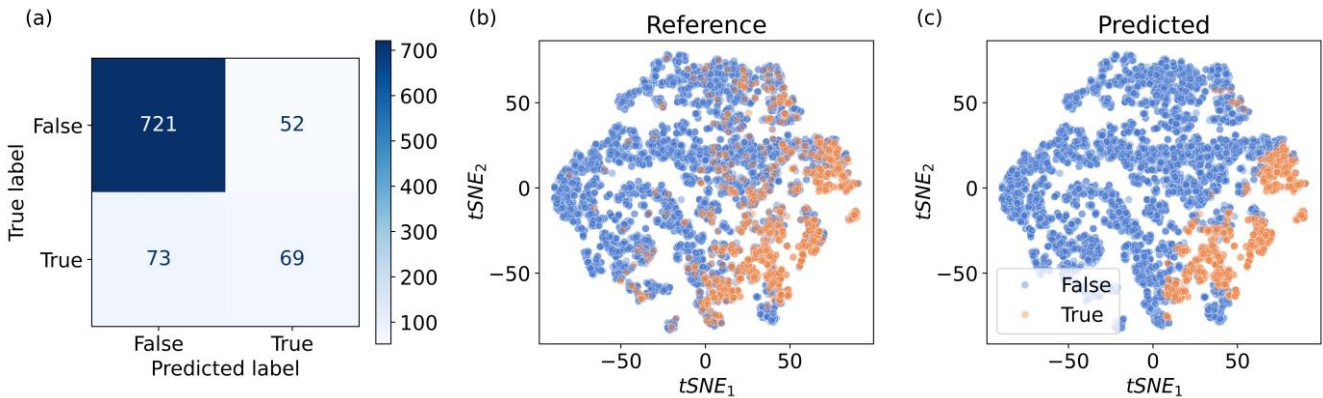


Figure 6. Classification of sr-mmp data from Tox21 dataset: a) Confusion matrix of predicted labels on the test set. b) t-SNE feature representation of the entire reference dataset according to their labels. c) Feature representation of the predicted labels.

Similarly, the analysis of results for the BACE, BBBP, ClinTox, HIV and SIDER datasets is presented in Appendix B. Overall, the binary classification results of our model for organic compounds exemplify its exceptional efficiency in predicting the behavior of interactions between organic compounds and protein molecules. By accurately classifying these compounds, our model provides valuable insights into their potential effects and interactions within biological systems. This capability holds significant promise for drug discovery, as it enables the identification of organic compounds that have a high likelihood of binding to specific protein targets and exerting desired therapeutic effects.

4 Discussion

One key aspect contributing to the success of the elEmBERT model is its ability to capture the complex geometric attributes inherent in chemical structures, which facilitates accurate prediction of multiple chemical properties. Our elEmBERT-V0 model is similar to previous proven models, like MolBERT [48] or MolBART [49]. These models use SMILES as input data for molecular representations. However, in chemistry-related tasks, it is important to consider information about the spatial distribution of atoms within compounds. Traditional text-based (SMILES) models are inherently unable to capture important structural and conformational details of compounds. This limitation is a significant drawback of such models. Our elEmBERT-V1 model effectively addresses and mitigates this drawback.

Transforming atomic PDFs into sub-elements and using their corresponding embedding vectors as inputs to the neural network ensures a comprehensive consideration of both local atomic and global compound features. This holds particular significance in the context of the "structure to property" task, where a thorough understanding of the atomic environment proves essential for the accurate prediction of compound properties. As has been shown in the LA task, the V1 model is excellent at capturing the geometric subtleties inherent in chemical structures, and this characteristic observation extends to the other datasets. As an example, we can consider the visualization of the attention scores of the last layer from the V0 and V1 models. Fig. 7 displays color-coded values of attention scores for materials containing Si and Osmium (Os) atoms. As can be seen, the V0 model assigns the same values for Si and Os atoms. In contrast, the V1 model, after the Km layer, Si and Os atoms were divided into two (Si^0, Si^5) and three subgroups ($\text{Os}^2, \text{Os}^4, \text{Os}^6$) respectively. Following this, the V1 model allocates diverse attention scores to individual sub-element atoms, thereby expanding the model's parameters and increasing its predictive performance.

Despite sufficient performance on inorganic datasets, our model shows a predictive gap compared to other models on the drug-related BACE and BBBP datasets. This discrepancy can be attributed to conformational variations among compounds present in these datasets. Although we transformed SMILES into 3D structures, the existence of multiple conformers for a given SMILES structure introduces complexities. Not all conformers generated in this study may precisely match the actual structural configuration, thus diminishing the predictive power of the model.

These issues may also account the minor prediction differences observed between the V0 and V1 models in organic benchmarks. To address these challenges, increasing the number of sub-elements can be increased, which may help to capture the complexity of the organic structures more effectively.

Furthermore, including positional information for uniformly described databases could further improve the predictive accuracy of our workflow (see Appendix C).

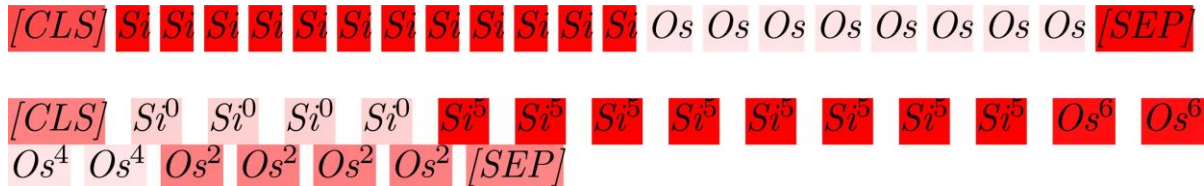


Figure 7. Visualization of the attention scores from elEmBERT. The top row displays the output from V0 and the bottom row the one from the V1 model.

5 Conclusions

In conclusion, the deep learning model presented in this paper signifies a marked advancement in the application of machine learning to computational chemistry. By integrating the attention mechanism and a transformer-based approach, our model can capture both local and global properties of chemical compounds, enabling highly accurate predictions of chemical properties that outperform similar approaches. The combination of principal component analysis and k-means clustering for sub-elements accounts for the nuanced effects stemming from electronic structure, a fact confirmed through the analysis of numerous chemical databases. Our classification approach, which relies on compound embeddings results in a substantially improved prediction accuracy compared to previously published scores. Additionally, t-SNE projections provide valuable insights into the classification mechanisms and can pinpoint sources of erroneous predictions. Future enhancements can likely be attained through augmentation of the sub-elements in the elEmBERT-V1 model and by the use of more sophisticated atomic descriptors.

Acknowledgements

The work has partially been carried out within the framework of the EUROfusion Consortium and received funding from the Euratom research and training programme by Grant Agreement No. 101052200-EUROfusion. The views and opinions expressed herein do not necessarily reflect those of the European Commission. The computational results have been obtained using the HPC infrastructure LEO of the University of Innsbruck.

Data availability

All data used in this paper are publicly available and can be accessed from various sources. The structure files for the MP metallicity dataset are accessible at <https://matbench.materialsproject.org/>. The LA, SG, and DIM datasets are available at

<https://github.com/sbanik2/CEGANN/tree/main/pretrained>. The BACE, BBBP, Clintox, HIV, and SIDER datasets can be retrieved from <https://moleculenet.org/>. Structure files for the Tox21 dataset can be obtained from <https://tripod.nih.gov/tox21/challenge/data.jsp>. The source code used in this study is available at <https://github.com/dmamur/elembert>, and detailed Python notebooks for replicating all calculations can be found on the corresponding GitHub page.

References

- [1] Ng M-F, Zhao J, Yan Q, Conduit G J and Seh Z W 2020 Predicting the state of charge and health of batteries using data-driven machine learning *Nat. Mach. Intell.* **2** 161–70
- [2] Liu Y, Guo B, Zou X, Li Y and Shi S 2020 Machine learning assisted materials design and discovery for rechargeable batteries *Energy Storage Mater.* **31** 434–50
- [3] Sawant V, Deshmukh R and Awati C 2023 Machine learning techniques for prediction of capacitance and remaining useful life of supercapacitors: A comprehensive review *J. Energy Chem.* **77** 438–51
- [4] Iwasaki Y, Takeuchi I, Stanev V, Kusne A G, Ishida M, Kirihara A, Ihara K, Sawada R, Terashima K, Someya H, Uchida K ichi, Saitoh E and Yorozu S 2019 Machine-learning guided discovery of a new thermoelectric material *Sci. Rep.* **9** 1–7
- [5] Akhter M N, Mekhilef S, Mokhlis H and Shah N M 2019 Review on forecasting of photovoltaic power generation based on machine learning and metaheuristic techniques *IET Renew. Power Gener.* **13** 1009–23
- [6] Toyao T, Maeno Z, Takakusagi S, Kamachi T, Takigawa I and Shimizu K 2020 Machine Learning for Catalysis Informatics: Recent Applications and Prospects *ACS Catal.* **10** 2260–97
- [7] Vamathevan J, Clark D, Czodrowski P, Dunham I, Ferran E, Lee G, Li B, Madabhushi A, Shah P, Spitzer M and Zhao S 2019 Applications of machine learning in drug discovery and development *Nat. Rev. Drug Discov.* **18** 463–77
- [8] Mikolov T, Chen K, Corrado G and Dean J 2013 Efficient estimation of word representations in vector space *1st Int. Conf. Learn. Represent. ICLR 2013 - Work. Track Proc.* 1–12
- [9] Tshitoyan V, Dagdelen J, Weston L, Dunn A, Rong Z, Kononova O, Persson K A, Ceder G and Jain A 2019 Unsupervised word embeddings capture latent knowledge from materials science literature *Nature* **571** 95–8

- [10] Hansen K, Biegler F, Ramakrishnan R, Pronobis W, Von Lilienfeld O A, Müller K R and Tkatchenko A 2015 Machine learning predictions of molecular properties: Accurate many-body potentials and nonlocality in chemical space *J. Phys. Chem. Lett.* **6** 2326–31
- [11] Jaeger S, Fulle S and Turk S 2018 Mol2vec: Unsupervised Machine Learning Approach with Chemical Intuition *J. Chem. Inf. Model.* **58** 27–35
- [12] Goh G B, Hodas N O, Siegel C and Vishnu A 2017 SMILES2Vec: An Interpretable General-Purpose Deep Neural Network for Predicting Chemical Properties
- [13] Zhang Y F, Wang X, Kaushik A C, Chu Y, Shan X, Zhao M Z, Xu Q and Wei D Q 2020 SPVec: A Word2vec-Inspired Feature Representation Method for Drug-Target Interaction Prediction *Front. Chem.* **7** 1–11
- [14] Stanev V, Oses C, Kusne A G, Rodriguez E, Paglione J, Curtarolo S and Takeuchi I 2018 Machine learning modeling of superconducting critical temperature *npj Comput. Mater.* **4**
- [15] Chen C, Ye W, Zuo Y, Zheng C and Ong S P 2019 Graph Networks as a Universal Machine Learning Framework for Molecules and Crystals *Chem. Mater.* **31** 3564–72
- [16] Kong S, Ricci F, Guevarra D, Neaton J B, Gomes C P and Gregoire J M 2022 Density of states prediction for materials discovery via contrastive learning from probabilistic embeddings *Nat. Commun.* **13** 1–12
- [17] Gori M, Monfardini G and Scarselli F 2005 A new model for earning in raph domains *Proc. Int. Jt. Conf. Neural Networks* **2** 729–34
- [18] Zhang S, Liu Y and Xie L 2020 Molecular Mechanics-Driven Graph Neural Network with Multiplex Graph for Molecular Structures *arXiv* **2011.07457** 1–14
- [19] Shui Z and Karypis G 2020 Heterogeneous molecular graph neural networks for predicting molecule properties *Proc. - IEEE Int. Conf. Data Mining, ICDM 2020-Novem* 492–500
- [20] Fung V, Zhang J, Juarez E and Sumpter B G 2021 Benchmarking graph neural networks for materials chemistry *npj Comput. Mater.* **7** 1–8
- [21] Xie T and Grossman J C 2018 Crystal Graph Convolutional Neural Networks for an Accurate and Interpretable Prediction of Material Properties *Phys. Rev. Lett.* **120** 145301
- [22] Guo Z, Zhang C, Yu W, Herr J, Wiest O, Jiang M and Chawla N V. 2021 Few-shot graph learning for molecular property prediction *Web Conf. 2021 - Proc. World Wide Web Conf.*

- [23] Bartók A P, Kondor R and Csányi G 2013 On representing chemical environments *Phys. Rev. B - Condens. Matter Mater. Phys.* **87** 1–16
- [24] Huo H and Rupp M 2022 Unified Representation of Molecules and Crystals for Machine Learning *Mach. Learn. Sci. Technol.* **3** 045017
- [25] Behler J 2021 Four Generations of High-Dimensional Neural Network Potentials *Chem. Rev.* **121** 10037–72
- [26] Unke O T and Meuwly M 2019 PhysNet: A Neural Network for Predicting Energies, Forces, Dipole Moments, and Partial Charges *J. Chem. Theory Comput.* **15** 3678–93
- [27] Vaswani A, Shazeer N, Parmar N, Uszkoreit J, Jones L, Gomez A N, Kaiser Ł and Polosukhin I 2017 Attention is all you need *Adv. Neural Inf. Process. Syst.* **2017-Decem** 5999–6009
- [28] Louis S Y, Zhao Y, Nasiri A, Wang X, Song Y, Liu F and Hu J 2020 Graph convolutional neural networks with global attention for improved materials property prediction *Phys. Chem. Chem. Phys.* **22** 18141–8
- [29] Billinge S J L 2019 The rise of the X-ray atomic pair distribution function method: A series of fortunate events *Philos. Trans. R. Soc. A Math. Phys. Eng. Sci.* **377**
- [30] Hjorth Larsen A, Jørgen Mortensen J, Blomqvist J, Castelli I E, Christensen R, Dułak M, Friis J, Groves M N, Hammer B, Hargas C, Hermes E D, Jennings P C, Bjerre Jensen P, Kermode J, Kitchin J R, Leonhard Kolsbjerg E, Kubal J, Kaasbjerg K, Lysgaard S, Bergmann Maronsson J, Maxson T, Olsen T, Pastewka L, Peterson A, Rostgaard C, Schiøtz J, Schütt O, Strange M, Thygesen K S, Vegge T, Vilhelmsen L, Walter M, Zeng Z and Jacobsen K W 2017 The atomic simulation environment—a Python library for working with atoms *J. Phys. Condens. Matter* **29** 273002
- [31] Shermukhamedov S, Mamurjonova D and Probst M 2023 Structure to Property: Chemical Element Embeddings and a Deep Learning Approach for Accurate Prediction of Chemical Properties *arXiv* **2309.09355** 1–11
- [32] Damm W, Frontera A, Rives J T and Jorgensen W L 1997 OPLS All-Atom Force Field for Carbohydrates *J. Comput. Chem.* **18** 1955–70
- [33] Gražulis S, Daškevič A, Merkys A, Chateigner D, Lutterotti L, Quirós M, Serebryanaya N

R, Moeck P, Downs R T and Le Bail A 2012 Crystallography Open Database (COD): an open-access collection of crystal structures and platform for world-wide collaboration *Nucleic Acids Res.* **40** D420–7

[34] Gražulis S, Chateigner D, Downs R T, Yokochi A F T, Quirós M, Lutterotti L, Manakova E, Butkus J, Moeck P and Le Bail A 2009 Crystallography Open Database – an open-access collection of crystal structures *J. Appl. Crystallogr.* **42** 726–9

[35] Jain A, Ong S P, Hautier G, Chen W, Richards W D, Dacek S, Cholia S, Gunter D, Skinner D, Ceder G and Persson K A 2013 Commentary: The materials project: A materials genome approach to accelerating materials innovation *APL Mater.* **1**

[36] Ong S P, Cholia S, Jain A, Brafman M, Gunter D, Ceder G and Persson K A 2015 The Materials Application Programming Interface (API): A simple, flexible and efficient API for materials data based on REpresentational State Transfer (REST) principles *Comput. Mater. Sci.* **97** 209–15

[37] Banik S, Dhabal D, Chan H, Manna S, Cherukara M, Molinero V and Sankaranarayanan S K R S 2023 CEGANN: Crystal Edge Graph Attention Neural Network for multiscale classification of materials environment *npj Comput. Mater.* **9** 1–12

[38] Ziletti A, Kumar D, Scheffler M and Ghiringhelli L M 2018 Insightful classification of crystal structures using deep learning *Nat. Commun.* **9** 1–10

[39] Wu Z, Ramsundar B, Feinberg E N, Gomes J, Geniesse C, Pappu A S, Leswing K and Pande V 2018 MoleculeNet: A benchmark for molecular machine learning *Chem. Sci.* **9** 513–30

[40] Kuhn M, Letunic I, Jensen L J and Bork P 2016 The SIDER database of drugs and side effects *Nucleic Acids Res.* **44** D1075–9

[41] O’Boyle N M, Banck M, James C A, Morley C, Vandermeersch T and Hutchison G R 2011 Open Babel *J. Cheminform.* **3** 1–14

[42] Anon RDKit: Open-source cheminformatics. <https://www.rdkit.org>

[43] Chollet F F and others 2015 Keras. GitHub, <https://github.com/keras-team/keras> (accessed May 1, 2024)

[44] Chen C and Ong S P 2021 AtomSets as a hierarchical transfer learning framework for small and large materials datasets *npj Comput. Mater.* **7**

[45] Li Y, Hsieh C-Y, Lu R, Gong X, Wang X, Li P, Liu S, Tian Y, Jiang D, Yan J, Bai Q, Liu H, Zhang S and Yao X 2022 GLAM : An adaptive graph learning method for automated molecular interactions and properties predictions *Nat. Mach. Intell.* **4** 645–51

[46] Li P, Li Y, Hsieh C-Y, Zhang S, Liu X, Liu H, Song S and Yao X 2021 TrimNet: learning molecular representation from triplet messages for biomedicine *Brief. Bioinform.* **22** bbaa266

[47] Baek J, Kang M and Hwang S J 2021 Accurate Learning of Graph Representations with Graph Multiset Pooling **1** 1–22

[48] Fabian B, Edlich T, Gaspar H, Segler M, Meyers J, Fiscato M and Ahmed M 2020 Molecular representation learning with language models and domain-relevant auxiliary tasks

[49] Irwin R, Dimitriadis S, He J and Bjerrum E J 2022 Chemformer: A pre-trained transformer for computational chemistry *Mach. Learn. Sci. Technol.* **3**

[50] Pedregosa F, Varoquaux G, Gramfort A, Michel V, Thirion B, Grisel O, Blondel M, Prettenhofer P, Weiss R, Dubourg V, Vanderplas J, Passos A, Cournapeau D, Brucher M, Perrot M and Duchesnay E 2011 Scikit-learn: Machine Learning in Python *J. Mach. Learn. Res.* **12** 2825–30

APPENDIX A

To categorize elements into sub-elements (Figure A1), we examined various unsupervised classification algorithms, including k-means, Feature Agglomeration, neural network encoder-decoder models (Figure A2), and Principal Component Analysis (PCA) of PDFs combined with the k-means algorithm. The number of clusters was determined based on the oxidation states of the elements, as detailed in Table A1.

Table A1. Cluster numbers (k) for clustering selected based on element (El) oxidation states.

<i>N</i>	<i>El</i>	<i>k</i>												
1	H	3	17	Cl	9	33	As	5	49	In	4	65	Tb	4
2	He	2	18	Ar	2	34	Se	6	50	Sn	4	66	Dy	3
3	Li	2	19	K	3	35	Br	7	51	Sb	4	67	Ho	2
4	Be	3	20	Ca	3	36	Kr	2	52	Te	6	68	Er	2
5	B	4	21	Sc	4	37	Rb	3	53	I	7	69	Tm	3
6	C	9	22	Ti	5	38	Sr	3	54	Xe	5	70	Yb	3
7	N	9	23	V	7	39	Y	4	55	Cs	3	71	Lu	2
8	O	5	24	Cr	9	40	Zr	5	56	Ba	2	72	Hf	4
9	F	2	25	Mn	11	41	Nb	6	57	La	3	73	Ta	6
10	Ne	2	26	Fe	9	42	Mo	9	58	Ce	4	74	W	9
11	Na	3	27	Co	7	43	Tc	10	59	Pr	4	75	Re	10
12	Mg	3	28	Ni	6	44	Ru	10	60	Nd	3	76	Os	10
13	Al	4	29	Cu	5	45	Rh	8	61	Pm	2	77	Ir	11
14	Si	9	30	Zn	3	46	Pd	3	62	Sm	3	78	Pt	5
15	P	9	31	Ga	4	47	Ag	5	63	Eu	3	79	Au	6
16	S	9	32	Ge	6	48	Cd	3	64	Gd	4	80	Hg	4
												96	Rn	1

Clustering was performed using structures from the Crystallography Open Database with the scikit-learn package [50]. This process involved calculating and extracting atomic probability density functions (PDFs) from all structures in the database. These PDFs were then aggregated according to atomic type to form the input data arrays. The models obtained from this clustering process were subsequently integrated into the elEmBERT model. Benchmark values for different classification methods are presented in Table A2, while visual differences in predicting sub-element indices among these methods are illustrated in Figures A3 and A4.

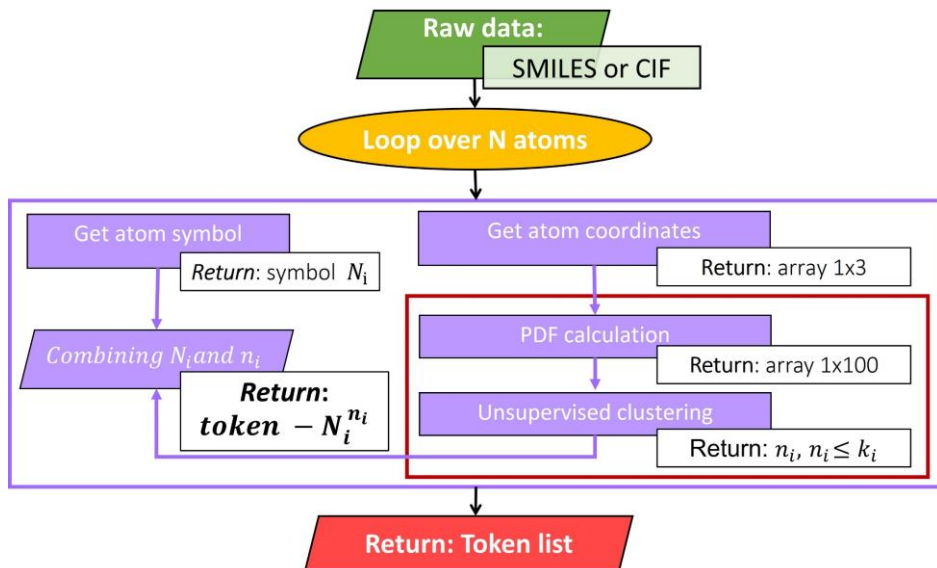


Figure A1. Workflow of the unsupervised classification module. The process starts with compounds provided in Crystallographic Information File (CIF) or SMILES format as input data. The module first extracts the atomic symbols and Cartesian coordinates of all atoms from this input. Next, PDFs are computed based on these coordinates. The computed PDFs are then subjected unsupervised clustering. The resulting clusters are mapped to the atomic symbols, facilitating their conversion into tokens for further analysis.

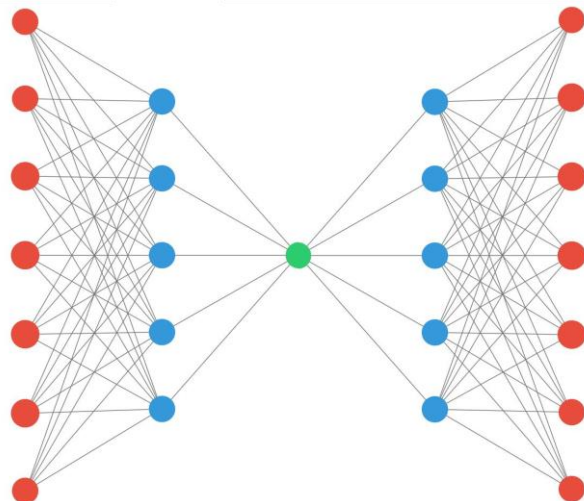


Figure A2. Schematic of a neural network for the encoding-decoding approach. This model is symmetric and aims to approximate the input data through a series of progressively reduced layers. The central layers (bottleneck layers), are configured with a number of neurons corresponding to the number of clusters specified in Table A1. As the input atom PDF traverses through the network, the model seeks to identify the neuron in these central layers that yields the highest activation value. This process allows the model to determine the cluster to which the input atom is assigned.

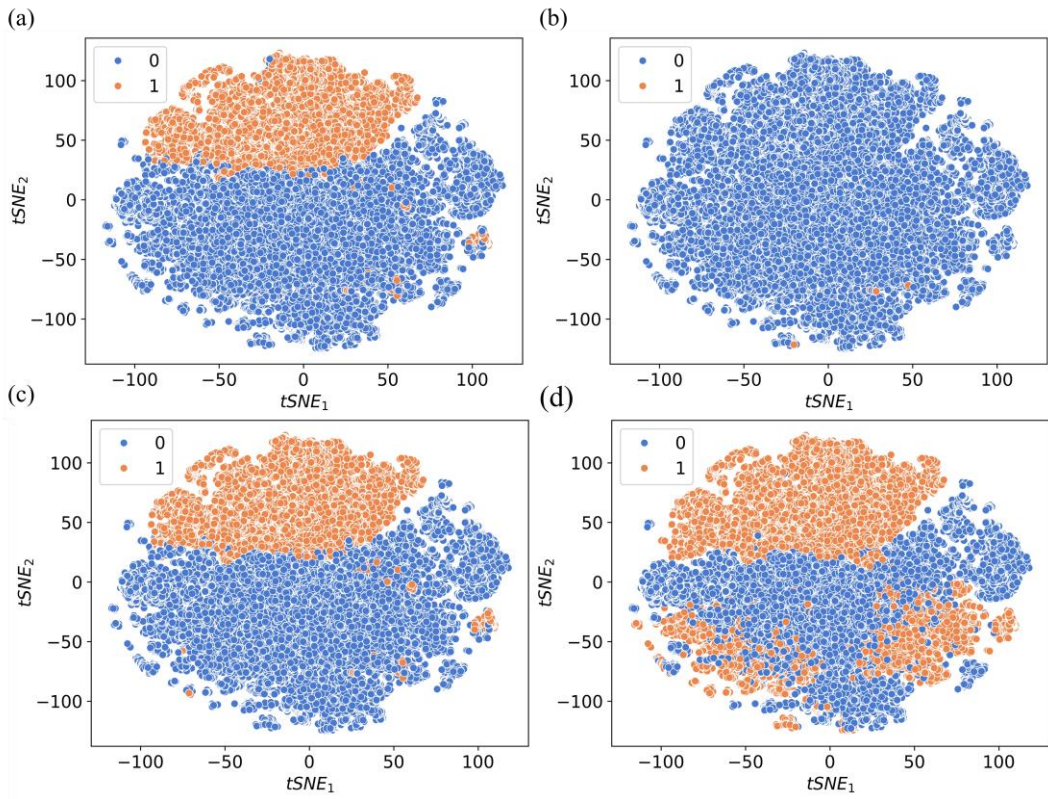


Figure A3. Sub-element classification and t-SNE Plots for Li for k_{means} (a), Feature Agglomeration (b), NN encoder-decoder (c) and PCA- k_{means} (d) algorithms.

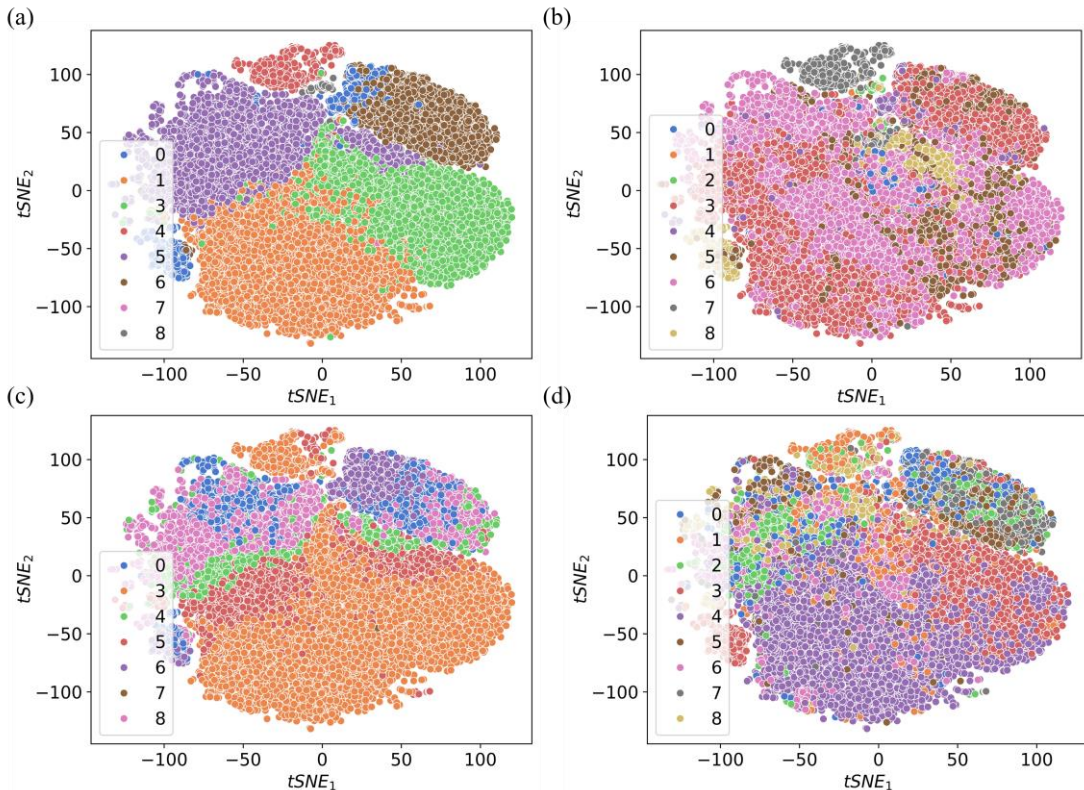


Figure A4. Sub-element classification and t-SNE Plots for Chlorine for k_{means} (a), Feature Agglomeration (b), NN encoder-decoder (c) and PCA- k_{means} (d) algorithms.

Table A2. Performance of different classification models applied to datasets (Matbench to TOXIC21) used in this work.

BENCHMARK	KM	NN	FA	PCA
MP METALLICITY	0.967	0.969	0.967	0.967
SG	0.954	0.954	0.953	0.967
LA	0.987	0.988	0.988	0.987
DIM	0.881	0.948	0.950	0.932
BACE	0.871	0.856	0.817	0.845
BBBP	0.887	0.893	0.924	0.896
CLINTOX	0.973	0.969	0.970	0.967
HIV	0.978	0.979	0.977	0.977

APPENDIX B

BACE

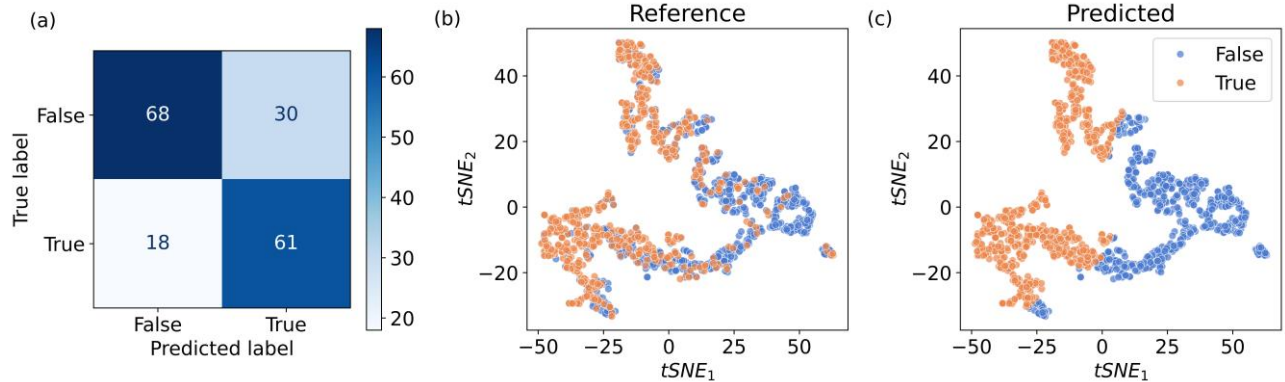


Figure B1. Classification of BACE data: a) Confusion matrix of predicted labels on the test set. b) t-SNE feature representation of the entire reference dataset according to their labels. c) Feature representation of the predicted labels.

BBBP

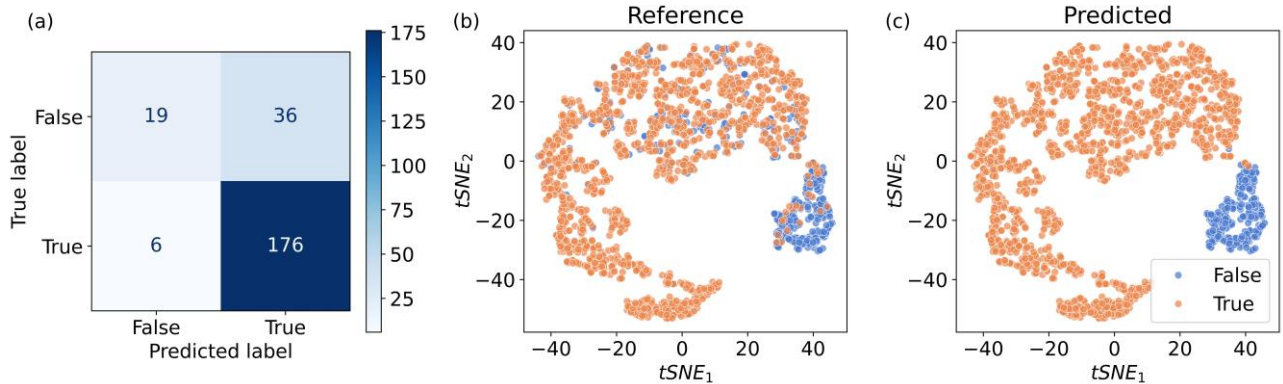


Figure B2. Classification of BBBP data: a) Confusion matrix of predicted labels on the test set. b) t-SNE feature representation of the entire reference dataset according to their labels. c) Feature representation of the predicted labels.

Clintox

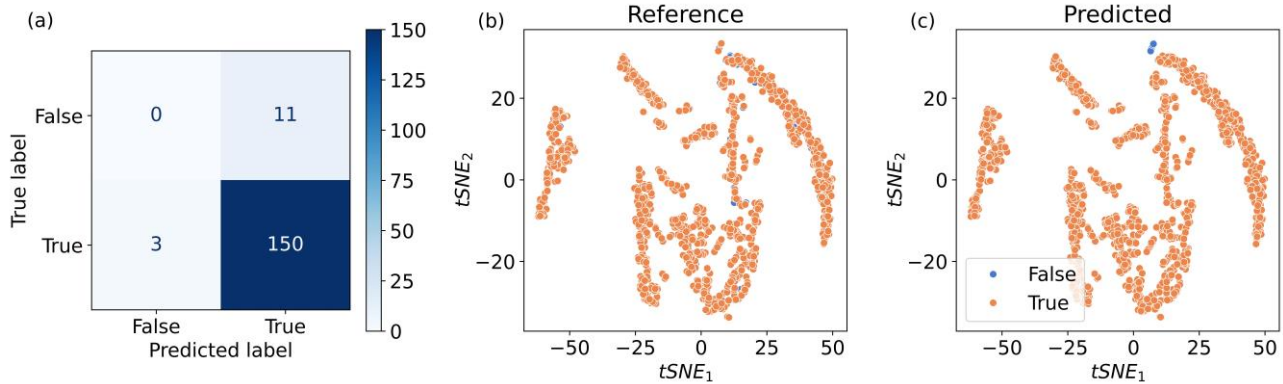


Figure B4. Classification of ClinTox FDA approval task: a) The confusion matrix of predicted labels on the test set. b) The t-SNE feature representation of the entire reference dataset according to their labels. c) The feature representation of the predicted labels.

HIV

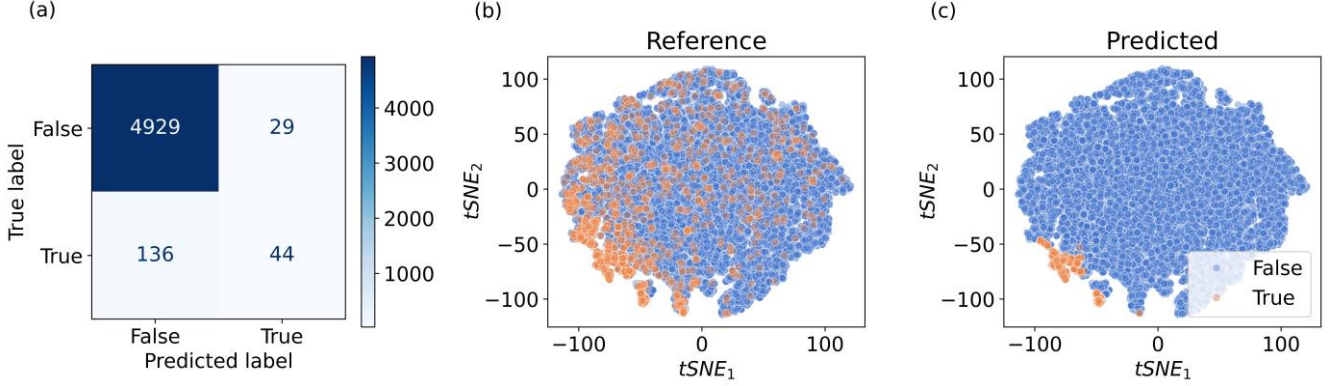


Figure B3. Classification of HIV data: a) Confusion matrix of predicted labels on the test set. b) t-SNE feature representation of the entire reference dataset according to their labels. c) Feature representation of the predicted labels.

SIDER

Table B1. ROC-AUC performances of various models on the SIDER dataset. MMGNN denotes the prior top-performing results [22]. The last column presents the elEmBERT model's average performance across all tasks. The Bold entries signify the highest performance, while underlined values indicate the second-best performance.

SIDER N	1	2	3	4	5	6	7	8	9	10	11	12	13	14
V0	0.684	0.709	0.985	0.676	0.847	0.738	0.945	0.839	0.739	0.634	0.775	0.908	0.819	0.853
V1	0.663	<u>0.707</u>	<u>0.983</u>	<u>0.689</u>	<u>0.838</u>	0.744	<u>0.941</u>	<u>0.832</u>	<u>0.724</u>	<u>0.613</u>	<u>0.760</u>	<u>0.892</u>	<u>0.816</u>	<u>0.849</u>
MMGNN	0.754	0.693	0.723	0.744	0.817	<u>0.741</u>	-	-	-	-	-	-	-	-
SIDER N	15	16	17	18	19	20	21	22	23	24	25	26	27	Ave
V0	0.809	<u>0.723</u>	0.926	<u>0.822</u>	<u>0.724</u>	<u>0.759</u>	0.764	<u>0.700</u>	0.927	<u>0.598</u>	0.747	0.925	0.698	0.778
V1	<u>0.782</u>	0.737	<u>0.917</u>	0.833	0.736	0.772	<u>0.726</u>	0.708	<u>0.923</u>	0.599	<u>0.742</u>	<u>0.916</u>	<u>0.684</u>	<u>0.773</u>
MMGNN	-	-	-	-	-	-	-	-	-	-	-	-	-	0.747

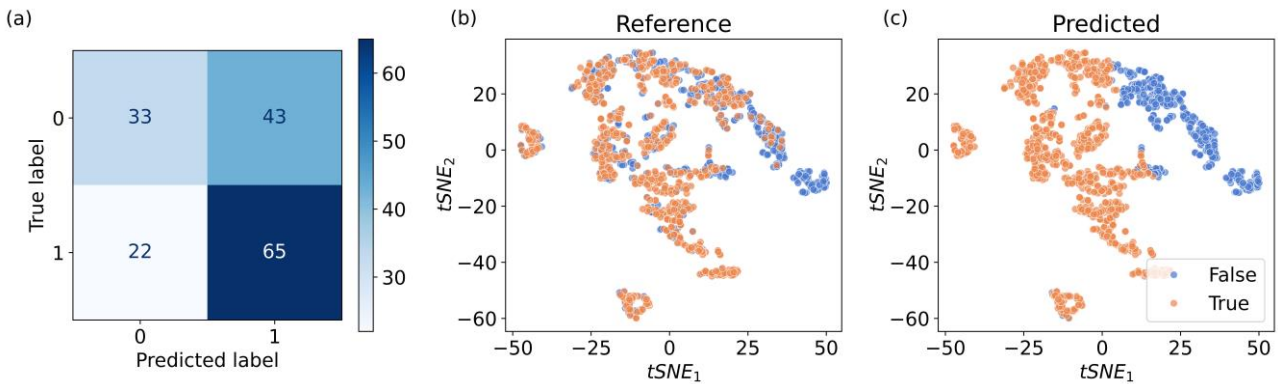


Figure B5. Classification of SIDER-1 data: a) Confusion matrix of predicted labels on the test set. b) t-SNE feature representation of the entire reference dataset according to their labels. c) Feature representation of the predicted labels.

Appendix C

In chemistry, the order of atoms in structures sometimes could be important, especially if a set of structures was generated or described in the same way. If the input sequence follows specific rules and order, positional encoding can capture additional information and enhance prediction quality. Comparing our property predictions with and without positional embeddings, we find that the former indeed enhances the accuracy of the predictions. The results are outlined in Table C1.

Table C1. ROC-AUC values for elEmBERT-V1 model. The P^+ column shows predictions for the test set with positional encoding, while the P^- column displays predictions without positional encoding.

BENCHMARK	P^+	P^-
MP METALLICITY	0.965	0.966
SG	0.968	0.966
LA	0.980	0.969
DIM	0.958	0.958
BACE	0.856	0.808
BBBP	0.905	0.888
CLINTOX	0.951	0.946
HIV	0.979	0.980